Supporting Information

Schito et al. 10.1073/pnas.1214019109

SI Materials and Methods

Orthotopic Transplantation of Human Breast Cancer Cells. All animal studies were approved by the Johns Hopkins University Animal Care and Use Committee and conformed to the Guide for the Care and Use of Laboratory Animals (1). Two million MDA-MB-231 or MDA-MB-435 cells were resuspended in 100 μL of a 4-mg/mL suspension of Matrigel (B&D) and were injected into the second (in cranial-to-caudal direction) left mammary gland of 5-wk-old female SCID mice (National Cancer Institute) under ketamine/xylazine anesthesia. Imatinib (Biovision) stock solution was prepared in DMSO and diluted in saline for i.p. administration at a dose of 50 mg·kg^{-1}·d^{-1}. Digoxin (Baxter) was administered i.p. at 2 mg·kg^{-1}·d^{-1} or 1 mg/kg twice daily. Primary tumors and ipsilateral axillary lymph nodes (LNs) were excised from mice, fixed in 10% neutral-buffered formalin, and submitted for sectioning and staining with H&E.

Cell Culture. MDA-MB-231, MDA-MB-435, and HeLa cells were cultured in high-glucose DMEM containing 10% FBS and 1% penicillin/streptomycin. ShRNA-transduced MDA-MB-231 cells were maintained in the presence of 0.5 μg/mL of puromycin. Human lymphatic endothelial cells (Lonza) were cultured in EGM2-MV medium at a starting density of 5,000 cells/cm^2. Cells were exposed to hypoxia at 37 °C in a modular chamber (Billups-Rothenberg) flushed with a gas mixture containing 1% O_2, 5% CO_2, and 94% N_2 (vol:vol:vol).

Immunoblot Assays. Aliquots of cell lysates (50–80 μg of total protein) were subjected to 10% SDS/PAGE, and immunoblots were probed with anti-platelet-derived growth factor B (PDGF-B) antibody (Novus Biologicals) at 1:2,500 dilution. HRP-conjugated anti-actin antibody (Santa Cruz) was used as loading control. Signal was visualized using the ECL detection system (Amersham).

Reverse Transcription and Quantitative Real-time PCR. RNA was extracted using TRIzol (Invitrogen), precipitated with isopropanol, treated with DNase I (Ambion), and reverse transcribed with the iScript cDNA Synthesis kit (Bio-Rad). Reverse transcription quantitative real-time PCR (RT-qPCR) was performed using Maxima SYBR Green Master Mix (Fermentas) and the iCycler Real-time PCR Detection System (BioRad). Optimal annealing temperature of primer pairs (Table S2) was determined by gradient PCR. The comparative $\Delta\Delta C_q$ method was used to calculate the relative expression of genes of interest in all experimental conditions (2). Results were normalized to the 18S rRNA signal.

Flow Cytometry. Cultured cells were detached with 1 mM EDTA in PBS, fixed in 2% paraformaldehyde, permeabilized, and incubated with rabbit polyclonal anti–PDGF-B, anti-PDGFRβ (Novus), and anti–P-Y-PDGFRβ primary antibodies (Beckton Dickinson) and an Alexa Fluor 594-conjugated goat anti-rabbit secondary antibody (Invitrogen). Cells incubated only with the secondary antibody were used as negative controls. The number of positive cells and mean fluorescence intensities were quantified in a LSR-II flow cytometer (Becton Dickinson). A minimum of 30,000 events per biological replicate were acquired.

Cell-Cycle Analysis. Cell-cycle analysis was performed as previously described (3). Briefly, cultured cells were detached, fixed for 30 min, and stained in 50 μg/mL of propidium iodide. DNA content was determined in a LSR-II flow cytometer (Beckton Dickinson). At least 10,000 events per sample were acquired. Phases of the cell cycle were modeled using the Dean–Jett–Fox algorithm (4) or Watson pragmatic method (5).

ChIP. HeLa cells were incubated for 4 h in the presence of vehicle (0.01% DMSO) or 1 mM dimethyloxalylglycine (DMOG) and were fixed in 3.7% formaldehyde. The immunoprecipitating antibodies used were anti–HIF-1α (Santa Cruz) and anti–HIF-1β (Novus Biologicals). Anti-rabbit IgG (Millipore) was used as a negative control. Chromatin was recovered by phenol-chloroform extraction and ethanol-sodium acetate precipitation. Candidate HIF-1–binding sites in the *PDGFB* gene were analyzed by qPCR using appropriate primers (Table S3).

Histopathology. Histopathological analysis of mouse orthotopic xenografts and axillary LNs was done in a blinded fashion by two independent operators (L.S. and S.R.). Each lymph node section was scored for the presence of metastases using a semiquantitative scale considering the apparent area of each lymph node occupied by MDA-MB-231 and MDA-MB-435 cells. The correlation coefficient between the two operators was $r > 0.95$ ($P < 0.001$) with an average bias not statistically different between observers by Bland–Altman analysis (6). To confirm metastases further, slides were subjected to vimentin immunohistochemistry.

Immunohistochemistry. Tissue sections were rehydrated, and antigen retrieval (7) was performed in sodium citrate at pH 6. Endogenous peroxidase activity was quenched with 3% H_2O_2 and blocked in serum-free protein-blocking solution (Dako). Specimens were incubated with anti-vimentin (Sigma) or anti–podoplanin-1 (Novus Biologicals) primary antibodies. Human breast cancer biopsies were incubated with anti–HIF-1α, anti–PDGF-B, or anti-podoplanin primary antibody (Novus Biologicals). Normal breast tissues served as negative controls for HIF-1α, PDGF-B, and podoplanin. PDGF-B and podoplanin signal was developed with the streptavidin-biotin-HRP system (Dako) using 3,3′-diaminobenzidine as a chromogen. The HIF-1α signal was developed with a catalyzed signal amplification system (Dako). Sections stained with isotype-matched IgG served as negative controls. Nuclei were counterstained with Mayer's hematoxylin (Sigma).

Clinical Breast Cancer Specimens. Biopsies from 16 women, age 39–80 y, diagnosed with breast cancer at the Department of Oncological Surgery, Regina Elena Hospital, Rome, Italy, were examined by four experienced histopathologists in the Unità Organizzativa Complessa Anatomia, Istologia Patologica e Citodiagnostica, Istituto di Ricovero e Cura a Carattere Scientifico, Istituto Regina Elena, Rome, Italy. The specimens were diagnosed as invasive breast carcinoma and graded according to the Union for International Cancer Control (UICC, 2009) and the Scarff–Bloom–Richardson systems. All patients gave their informed consent for the study.

Digital Image Analysis. Immunohistochemical staining was quantified by thresholding the diaminobenzidine signal using a deconvolution algorithm (8, 9). Images were converted to binary pixel data, and the positive pixels were calculated as a fraction of the cross-sectional area occupied by tissue in each field using custom macros programmed in the ImageJ software (National Institutes of Health). The signal intensity of deconvoluted diaminobenzidine staining in human specimens was

quantified after calculation of a global threshold using the Otsu algorithm (10). After thresholding, pixel intensities were rescaled in a range between 0 and 1 arbitrary units. The mean signal intensity of positively immunostained areas was normalized to total tissue area. To compare signal intensities between HIF-1α and PDGF-B using multiple linear regression, the raw values were standardized and expressed as z-scores. The number of low-magnification fields (40×) varied according to the specimen analyzed but typically was three or four for LNs, six to eight for xenografts, and 8–15 for human breast cancer biopsies encompassing the total surface area of the histological sections. Lymphatic vessel area was calculated as the integrated luminal surface enclosed by podoplanin-positive pixels divided by the total number of vessels and was expressed as mean area per 100 vessels. All morphometric and intensity measurements in human biopsies were implemented as Matlab code (Mathworks). Area measurements were converted to square micromillimeters.

ShRNA-Mediated Knockdown of HIF-1α and HIF-2α. Complementary oligonucleotides encoding shRNAs directed against HIF-1α or HIF-2α were annealed and ligated into the pSUPER.retro.neo. GFPvector (OligoEngine). A scrambled shRNA with no significant homology to any mammalian gene also was prepared. An shRNA construct targeting PDGF-B and cloned into the pLKO.1 lentiviral vector was purchased from Sigma.

Migration Assay. Migration of human lymphatic endothelial cells was measured using a Boyden chamber assay with Transwell membranes (Corning). The conditioned medium produced by MDA-MB-231 subclones was collected and used as chemoattractant. Migrated cells were fixed in methanol and stained with

crystal violet. The optical density of each membrane was measured using the ImageJ software (National Institutes of Health).
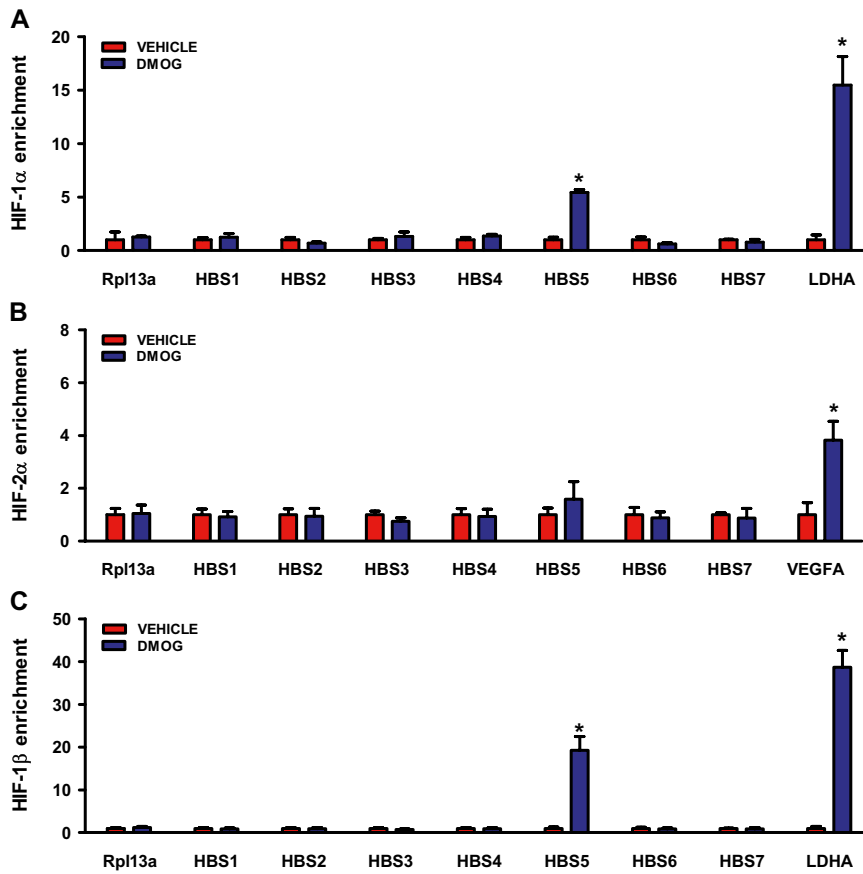
Luciferase Reporter Assay. The 39-bp sequence of the putative HIF-binding sequence HBS5, located +9,622 bp from the translation start site of the human *PDGFB* gene, was inserted into the *BglII* site of the pGL2-Promoter vector (Promega), which carries the coding sequence of firefly luciferase downstream of SV40 promoter sequences. HeLa cells (50,000 cells per well) were transiently cotransfected with 25 ng of pGL2 and 5 ng of the pSV-Renilla plasmid, which encodes *Renilla* luciferase downstream of SV40 promoter sequences, using PolyJet (SignaGen Laboratories). After 18 h, cells were incubated at 20% or 1% O_2 for 24 h. Firefly luciferase activity was measured with the dual luciferase reporter assay system (Promega) and normalized to *Renilla* chemiluminescence.

Data Analysis. All data were expressed as mean ± SEM. Normality of the data was tested with the D'Agostino–Pearson test. When data were not Gaussian, a logarithmic or square root transformation was applied. Differences between two experimental groups were assessed using Student's *t* test. Three or more groups were analyzed with one-, two-, or three-way ANOVA followed by post hoc comparisons with the Bonferroni or Holm–Sidak tests, according to the number of factors present in the data. Dose–response curves were modeled using a symmetrical sigmoidal function and nonlinear regression (11). IC_{50} values were obtained from fitted parameters. Multiple linear regression analysis was performed on morphometric and immunohistochemical signal intensity values from human breast cancer biopsies, followed by ANOVA and the Shapiro–Wilk test for normality. A two-tailed value of $P < 0.05$ was considered statistically significant.

1. Committee on Care and Use of Laboratory Animals (1996) *Guide for the Care and Use of Laboratory Animals* (Natl Inst Health, Bethesda), DHHS Publ No (NIH) 85–23.
2. Schmittgen TD, Livak KJ (2008) Analyzing real-time PCR data by the comparative C(T) method. *Nat Protoc* 3:1101–1108.
3. Riccardi C, Nicoletti I (2006) Analysis of apoptosis by propidium iodide staining and flow cytometry. *Nat Protoc* 1:1458–1461.
4. Fox MH (1980) A model for the computer analysis of synchronous DNA distributions obtained by flow cytometry. *Cytometry* 1:71–77.
5. Watson JV, Chambers SH, Smith PJ (1987) A pragmatic approach to the analysis of DNA histograms with a definable G1 peak. *Cytometry* 8:1–8.
6. Bland JM, Altman DG (1986) Statistical methods for assessing agreement between two methods of clinical measurement. *Lancet* 1:307–310.
7. Shi SR, Key ME, Kalra KL (1991) Antigen retrieval in formalin-fixed, paraffin-embedded tissues: An enhancement method for immunohistochemical staining

based on microwave oven heating of tissue sections. *J Histochem Cytochem* 39:741–748.
8. Rey S, Corthorn J, Chacón C, Iturriaga R (2007) Expression and immunolocalization of endothelin peptides and its receptors, ETA and ETB, in the carotid body exposed to chronic intermittent hypoxia. *J Histochem Cytochem* 55:167–174.
9. Ruifrok AC, Johnston DA (2001) Quantification of histochemical staining by color deconvolution. *Anal Quant Cytol Histol* 23:291–299.
10. Otsu N (1979) A threshold selection method from gray-level histograms. *IEEE Trans Syst Man Cybern* 9:62–66.
11. DeLean A, Munson PJ, Rodbard D (1978) Simultaneous analysis of families of sigmoidal curves: Application to bioassay, radioligand assay, and physiological dose-response curves. *Am J Physiol* 235:E97–E102.

Fig. S1. HIF knockdown in breast cancer cells inhibits lymph node metastasis. MDA-MB-231 human breast cancer cells (BCCs), which were stably transfected with empty vector (EV), or vector encoding KD shRNA directed against HIF-1α (1αKD), HIF-2α (2αKD), or both (DKD), were orthotopically transplanted into the mammary fat pad of SCID mice. (*A*) H&E staining of axillary LNs ipsilateral to the tumors 24 d after transplantation. (*Upper*) Low magnification shows no gross alterations of LN morphology. (Scale bar, 500 μm) (*Lower*) High magnification shows clustered cells with marked anisokaryosis (white arrows) which contrasts with normal lymphocytes (yellow arrows). (Scale bar, 50 μm.) (*B*) Quantification of LN invasion was performed in a blinded fashion using a histopathological score to assign grades of invasion according to the cross-sectional area occupied by BCCs as follows: 0, 0%; 1, <25%; 2, 25–50%; 3, 50–75%; 4, 75–100%. *$P <$ 0.05 vs. EV by Bonferroni test after one-way ANOVA. Data are expressed as mean $\pm$ SEM ($n = 5$).

A   **Axillary lymph node**

H&E   Vimentin

B   **Primary tumor - Vimentin**

EV   1αKD

2αKD   DKD

C

r= 0.8945
$P < 0.0001$

Vimentin$^+$ area ($\mu m^2 \times 10^3$) vs Histopathology score

Fig. S2. Correlation between histopathological score and vimentin immunohistochemistry for detection of LN metastasis. (*A*) Representative image of an axillary LN section analyzed for the presence of human breast cancer metastases by H&E staining (*Left*) followed by destaining and immunostaining for human vimentin (*Right*). (Scale bar, 100 μm.) (*B*) Representative immunohistochemistry for vimentin in 1αKD, 2αKD, DKD, or EV orthografts showing similar signal intensities. (Scale bar, 200 μm.) (*C*) Linear regression showing the relationship between the vimentin-positive area and the clinical histopathology score.

Fig. S3. ChIP assays for HIF-binding sites in the *PDGFB* gene. Chromatin from cells exposed to vehicle (red) or DMOG (blue) for 4 h was precipitated with antibodies directed against HIF-1α (*A*), HIF-2α (*B*), or HIF-1β (*C*). The non-HIF target gene *RPL13A* was used as a negative control, and *LDHA* or *VEGFA* was used as a positive control for binding of HIF-1α or HIF-2α, respectively. *LDHA* also was used as a positive control for HIF-1β binding. *$P < 0.05$ DMOG vs. vehicle by Bonferroni test after two-way ANOVA. Data are expressed as mean ± SEM ($n = 3$).
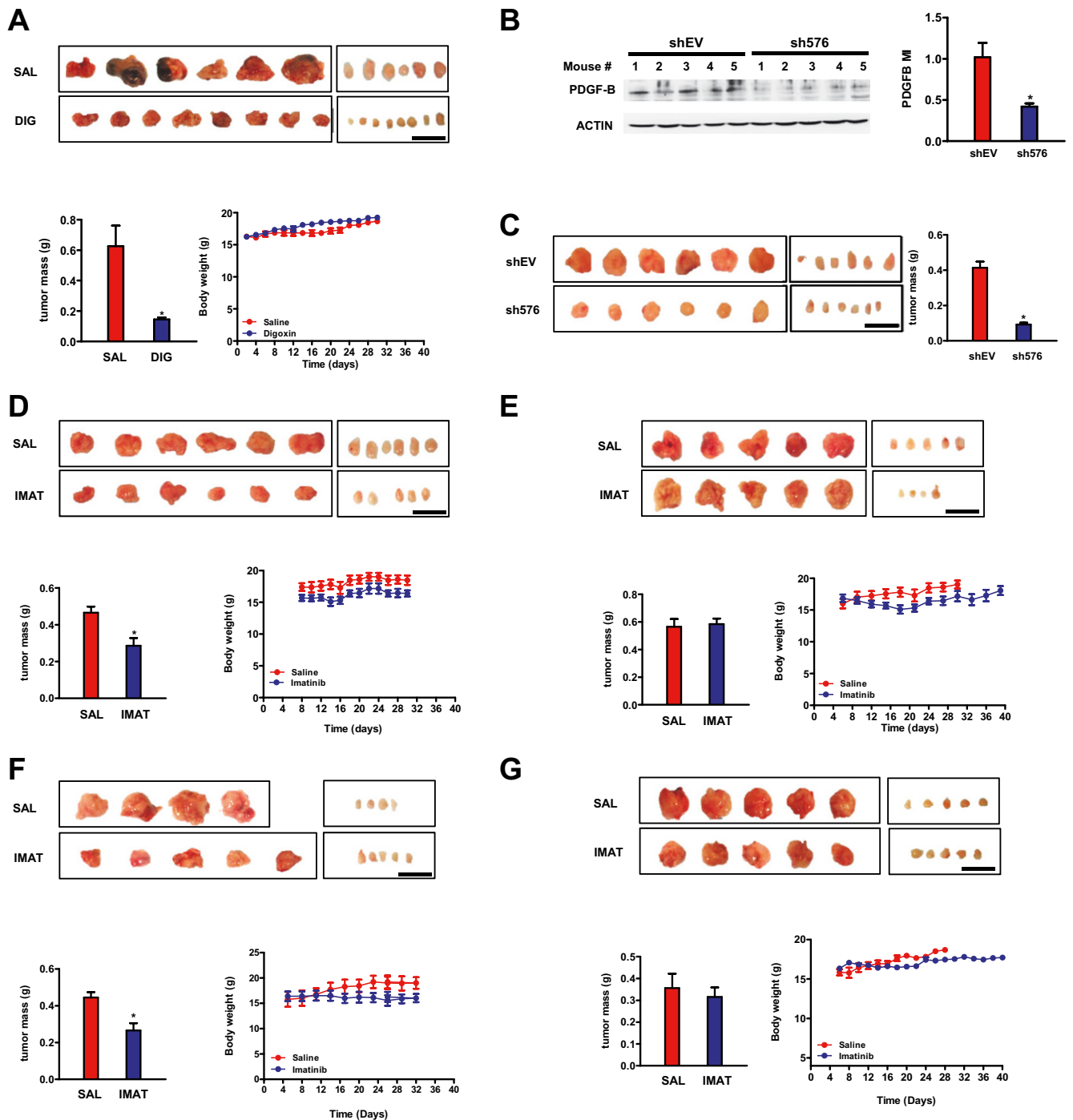
Fig. S4. Effect of digoxin, imatinib, and PDGF-B genetic knockdown on body weight, BCC orthografts, and lymph nodes of SCID mice. (*A*) (*Upper*) MDA-MB-231 orthografts from mice treated with saline (SAL) or digoxin (DIG) for 28 d were excised and photographed. Axillary LNs are shown to the right of tumor images. (*Lower*) Effect of digoxin treatment on tumor mass and body weight. (*B*) Immunoblot assay of PDGF-B in orthografts from shEV and sh576 tumor-bearing mice harvested 30 d postimplantation (*Left*) and densitometric analysis (*Right*). (*C*) MDA-MB-231 orthografts excised from shEV and sh576 tumor-bearing mice showing differences in volume (*Left*) and mass (*Right*). Axillary LNs are shown to the right of tumor images. (*D*) (*Upper*) MDA-MB-231 orthografts were excised from mice treated with saline or imatinib (IMAT) for 22 d. Axillary LNs are shown to the right of tumor images. (*Lower*) Effect of imatinib treatment on tumor mass and body weight is shown. (*E*) (*Upper*) MDA-MB-231 orthografts excised from mice treated with saline or imatinib for 24 or 33 d postimplantation, respectively. Axillary LNs collected are shown to the right of the tumor images. (*Lower*) Effect of imatinib treatment on tumor mass and body weight is shown. (*F*) (*Upper*) MDA-MB-435 orthografts were excised from mice treated with saline or imatinib for 27 d. Axillary LNs are shown to the right of tumor images. (*Lower*) Effect of imatinib treatment on tumor mass and body weight is shown. (*G*) (*Upper*) MDA-MB-435 orthografts excised from mice treated with saline or imatinib for 22 or 36 d postimplantation, respectively. Axillary LNs are shown to the right of the tumor images. (*Lower*) Effect of imatinib treatment on tumor mass and body weight is shown. $*P < 0.05$ vs. saline or shEV as appropriate by Bonferroni post hoc tests after two-way ANOVA or Student's *t* test. Data are expressed as mean $\pm$ SEM. (Scale bars, 10 mm for tumors and 500 μm for LNs.)

Fig. S5. Absence of lung metastases in tumor-bearing mice. MDA-MB-231 (*A*) or MDA-MB-435 (*B*) cells were injected into the mammary fat pad of female SCID mice and allowed to grow to similar volumes (~800–900 μm^3). Lungs were excised, submitted for H&E staining, and examined for the presence of metastatic foci. No distant metastases were found by histopathological examination 28 or 42 d posttransplantation in saline (SAL)- or imatinib (IMAT)- treated mice. (*Left* and *Center*) Low magnification. (Scale bars, 200 μm.) (*Right*) High magnification. (Scale bars, 50 μm.)

Table S1.   Clinical characteristics of 16 women diagnosed with breast cancer

Age (y)	63 (range,39–80)
Histological type	
Invasive lobular carcinoma	2 (13%)
Invasive ductal carcinoma	14 (88%)
UICC tumor stage	
pT_1	8 (50%)
pT_2	6 (38%)
pT_3	0 (0%)
pT_4	1 (6%)
pT_X	1 (6%)
Nodal status	
N_0	6 (38%)
N_1	3 (19%)
N_2	1 (6%)
N_3	1 (6%)
N_X	5 (31%)
Grade (Scarff–Bloom–Richardson)	
G_1	2 (13%)
G_2	8 (50%)
G_3	6 (38%)
Sentinel node	
Positive	2 (13%)
Negative	5 (31%)
Unknown	9 (56%)
One-step nucleic acid amplification, for detection of cytokeratin mRNA	
Positive	3 (19%)
Negative	3 (19%)
Unknown	10 (63%)
Free margin	
Present	0 (0%)
Absent	16 (100%)
Immunohistochemical staining	
HIF-1α–positive	16 (100%)
PDGF-B–positive	15 (94%)
HIF-1α /PDGF-B double positive	15 (94%)

Table S2. Forward and reverse primers used for qPCR

Target	Primer sequences	National Center for Biotechnology Information RefSeq
18S rRNA	Forward: CGGCGACGACCCATTCGAAC	NR_003286
	Reverse: GAATCGAACCCTGATTCCCCGT	
BNIP3	Forward: AACTCAGATTGGATATGGGATTGG	NM_004052
	Reverse: AGAGCAGCAGAGATGGAAGG	
GLUT1	Forward: CGGGCCAAGAGTGTGCTAAA	NM_006516
	Reverse: TGACGATACCGGAGCCAATG	
VEGFA	Forward: AACTTCTGGGCTGTTCTC	NM_001025366
	Reverse: TCCTCTTCCTTCTCTTCTTC	
VEGFC	Forward: CCACGGGAGGTGTGTATAG	NM_005429
	Reverse: AGGCACTGTAATTTCAAATAACG	
VEGFD	Forward: CTGCCTGATGTCAACTGCTTAG	NM_004469
	Reverse: TTCACTGGTCCATGTTCATTACTG	
PDGFA	Forward: TAAGCATGTGCCCGAGAAG	NM_002607
	Reverse: GACCTGACTCCGAGGAATC	
PDGFB	Forward: TTATGAGATGCTGAGTGACC	NM_002608
	Reverse: AACCCAGGCTCCTTCTTC	
PDGFC	Forward: TGGGATTATGTGGAAACTACC	NM_016205
	Reverse: CTTTGGAAGCAGCGACTC	
PDGFD	Forward: CGGCTCATCTTTGTCTACAC	NM_025208
	Reverse: CATCTCTTCGGTACAAGTCTG	
ANGPT1	Forward: TGGACTGTAATACAACATCGTG	NM_001199859
	Reverse: ACTGCCTCTGACTGGTAATG	
NRP2	Forward: GCAAGAATAGAGGTGAAGACAAG	NM_201266
	Reverse: CCCAGGTGAGAGGAAACATATC	
PGF	Forward: TGCTGCGGCGATGAGAATC	NM_002632
	Reverse: GTCTCCTCCTTTCCGGCTT	
IGF1	Forward: GGCTGACCAAGCTGAAACTC	NM_001111283
	Reverse: ATCGCTTAAACCCAGGAGGT	
IGF2	Forward: AACCCCCAAATTTCATGTCA	NM_000612
	Reverse: TGCGTTCTTGCTTTTGTCAC	
FGF2	Forward: GGTGAAACCCCGTCTCTACA	NM_00200
	Reverse: TCTGTTGCCTAGGCTGGACT	
PDGFRβ	Forward: CTGCTGTTGCTGTCTCTC	NM_002609
	Reverse: AGAACGAAGGTGCTGGAG	
Hs-HK2	Forward: CCAGTTCATTCACATCATCAG	NM_000189.4
	Reverse: CTTACACGAGGTCACATAGC	

Table S3. Forward and reverse primers used for ChIP qPCR

Target	Primer sequences
RPL13A	Forward: GTGCAGGTCCTGGTGCTTGAT
	Reverse: GGCCCGGAAGTGGTAGGGG
HBS5	Forward: AGCTCACTCAGCGAATGG
	Reverse: AGGTTAGAATAGAATGGAATTTGC